

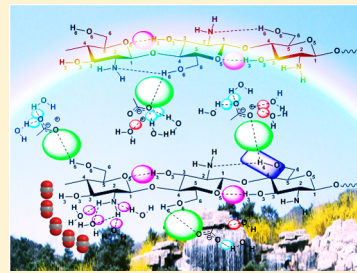
The Dynamic Process of Atmospheric Water Sorption in [EMIM][Ac] and Mixtures of [EMIM][Ac] with Biopolymers and CO₂ Capture in These Systems

Yu Chen, Xiaofu Sun, Chuanyu Yan, Yuanyuan Cao, and Tiancheng Mu*

Department of Chemistry, Renmin University of China, Beijing 100872, P. R. China

Supporting Information

ABSTRACT: There are mainly three findings related to the dynamic process of atmospheric water sorption in the ionic liquid (IL) 1-ethyl-3-methyl-imidazolium acetate ([EMIM][Ac]) and its mixtures with biopolymers (i.e., cellulose, chitin, and chitosan), and CO₂ capture in these systems above. The analytical methods mainly include gravimetric hygroscopicity measurement and in situ infrared spectroscopy with the techniques of difference, derivative, deconvoluted attenuated total reflectance and two-dimensional correlation. These three findings are listed as below. (1) Pure [EMIM][Ac] only shows a two-regime pattern, while all the mixtures of [EMIM][Ac] with biopolymers (i.e., cellulose, chitin, and chitosan) present a three-regime tendency for the dynamic process of atmospheric water sorption. Specifically, the IL/chitosan mixture has a clear three-regime mode; the [EMIM][Ac]/chitin mixture has an unclear indiscernible regime 3; and the [EMIM][Ac]/cellulose mixture shows an indiscernible regime 2. (2) [EMIM][Ac] and its mixtures with biopolymers could physically absorb a trace amount of and chemically react with a much larger amount of CO₂ from the air. The chemisorption capacity of CO₂ in these pure and mixed systems is ordered as chitosan/[EMIM][Ac] mixture > chitin/[EMIM][Ac] mixture > cellulose/[EMIM][Ac] mixture > pure [EMIM][Ac] (ca. 0.09 mass ratio % g/g CO₂/IL). (3) The CO₂ solubility in [EMIM][Ac] decreases about 50% after being exposed to the atmospheric moist air for some specific time period.



1. INTRODUCTION

The fossil fuel resources (e.g., coal, oil, and natural gas) are overexploited, not renewable, and not environment-friendly. Consequently, the utilization of biorenewable, biocompatible, and abundant biopolymers (e.g., cellulose, chitin, and chitosan; Scheme 1) attracts enormous attention. Cellulose is the most abundant polysaccharide on Earth, which is extensively used in the fields of paper products, fibers, consumables, filtration media, biofuels, building materials, and miscellaneous materials. Chitin, the second abundant polysaccharide after cellulose, is widely applied in agriculture, industrial, medicine, and biomedical research.¹ Chitosan, a deacetylated derivative of chitin, has a range of applications in agriculture and horticultural uses, natural biocontrols and elicitors, water filtration, wine making, and fungal sources.¹ Unfortunately, these biopolymers are insoluble in common solvents (e.g., water, methanol, and acetonitrile). The traditional solvents for processing biopolymers suffer many drawbacks, such as high cost, difficulty in regeneration, obvious volatility, and inefficient solvation ability.

Thus, ionic liquids (ILs)² are suggested as promising solvents to dissolve biopolymers due to their low volatility, high thermal stability, low melting point, and high tunability.^{3,4} ILs have also been extensively used or studied in many other fields, such as drying materials or materials synthesis,^{5,6} gas-capturing/converting solvents/catalysts,^{7–16} relative humidity regulators,¹⁷ and iodine absorbents.¹⁸ Cellulose, chitin, and chitosan cannot be dissolved in conventional ILs (e.g., 1-butyl-3-methyl-

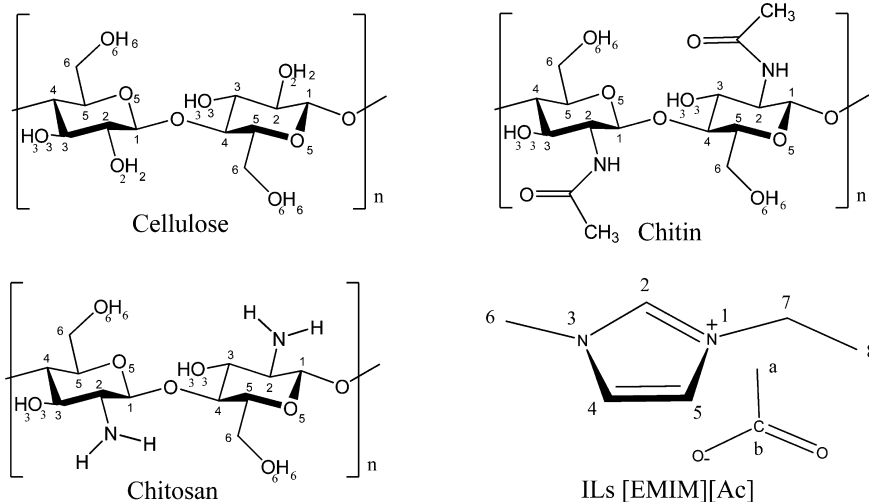
imidazolium tetrafluoroborate ([BMIM][BF₄]) and 1-butyl-3-methyl-imidazolium bis-trifluoromethylsulfonyl-imide ([BMIM][Tf₂N])).² Some halogen-containing ILs (e.g., [BMIM][Cl] and [AMIM][Cl]) show desirable solvation ability for cellulose but have negligible solubility for chitin and/or chitosan. Acetate-based ILs (AcILs, e.g., 1-ethyl-3-methyl-imidazolium acetate ([EMIM][Ac]) in Scheme 1 and 1-butyl-3-methyl-imidazolium acetate ([BMIM][Ac])) with the highly basic acetate anion are good solvents for cellulose, chitin, and chitosan at the same time. Furthermore, AcILs are more biodegradable, less viscous, and less toxic than most other ILs.

Regenerating biopolymers from mixtures of AcILs and biopolymers is presumed to be an imperative procedure.¹⁹ Water is one of the common, cheap, and efficient antisolvents to regenerate biopolymers from ILs.^{2,20–24} However, most of the reports focused on the manually added water in experiment. The ubiquitously and unavoidably atmospheric water effect on mixtures of biopolymers with ILs has never been reported. Nevertheless, nearly all the ILs possess the hygroscopicity feature.^{25–32} Even the anhydrous ILs, such as [BMIM][Tf₂N], could absorb a trace amount of water from moist air.^{33,34} Particularly, AcILs show a higher hygroscopicity tendency than other kinds of ILs,³⁴ possibly due to their much basic anion.³⁵ Furthermore, the presence of water in some other kinds of ILs

Received: September 9, 2014

Published: September 10, 2014

Scheme 1. Chemical Structure and Notation of Cellulose, Chitin, Chitosan, and [EMIM][Ac]



(with BF_4^- or PF_6^- anion) might produce detrimental gases, such as HF.³⁶ Structure,^{37–42} property,^{43–46} and application^{2,21,47} of ILs (including AcILs) could be influenced in different degrees after the introduction of water.

Thus, several questions are raised as below. How is the atmospheric water dynamically absorbed in pure AcILs and mixtures of biopolymers with AcILs? What are the differences among them, and why? Comparing the hygroscopicity of [BMIM][Ac] that is tethered with a longer alkyl chain length than [EMIM][Ac], we found a higher hygroscopicity for [EMIM][Ac] than [BMIM][Ac].⁵ Why does a shorter alkyl chain length on the cation imidazolium ring lead to an increase of hygroscopicity? Furthermore, AcILs tend to spontaneously form stable chemical complexes with CO_2 ,^{48–51} so it might be possible to capture a trace amount of CO_2 from the air, although the composition of CO_2 in the atmosphere is relative low, ca. 0.04 (vol. fra.) % or ca. 40 Pa. Actually, there are large quantities of reports on the CO_2 capture from the ambient air by other materials.^{52–55} However, could pure AcILs and mixtures of biopolymers with AcILs capture CO_2 from the atmospheric air? Could atmospheric water influence the CO_2 capture in AcILs? This paper is mainly aimed to discuss the above questions.

Generalized two-dimensional correlation spectroscopy (G-2D-COS) is applied to investigate the dynamic process of atmospheric water sorption in pure AcILs and mixtures of biopolymers with AcILs. Specifically, the G-2D-COS technique can be divided into synchronous (s-G-2D-COS) and asynchronous (as-G-2D-COS) modes. The correlation maps of s-G-2D-COS and as-G-2D-COS are symmetric and asymmetric with the diagonal line, corresponding to the coincidental and sequential changes of spectra intensity variations at two spectral variables, respectively.^{56–58} Advanced 2D-COS methods include autocorrelation moving-window 2D-COS (auto-MW2D-COS with s and as modes)⁵⁹ and perturbation-correlation MW2D-COS (PCM2D-COS, also with s and as modes),⁶⁰ because of their advantages in turning-points-seeking ability along the perturbation variable.^{60,61} Infrared spectroscopy (IR) is a powerful and sensitive tool to detect the molecular interactions among IL molecules or between ILs and other solvents, especially for an *in situ* investigation.^{29,62–64} The deconvolution, derivative, and difference of raw IR data could obtain more subtle information.

Thus, combination of 2D-COS and IR (i.e., 2D-COS-IR) and deconvolution, derivative, and difference IR are chosen to detect the dynamic sorption process of atmospheric water by the mixtures of AcILs with biopolymers in this paper. In the main text as to the 2D-COS IR spectra, we mainly report the PCM2D-COS analysis (including s-PCM2D-COS and as-PCM2D-COS), which is placed in the manuscript part (corresponding to Figures 2 and 3, respectively). Instead, G-2D-COS (including s-G-2D-COS and as-G-2D-COS) is reported in the Supporting Information (i.e., Figure S2). The reason for choosing PCM2D-COS rather than G-2D-COS as the main analyzing tool is that the PCM2D-COS technique is very helpful to capture the tipping point along the perturbation direction accurately. For example, by using PCM2D-COS spectra, Ozaki et al. found that a specific polymer has a glass-to-rubber transition temperature.⁶⁵ Richardson also got a clearer critical melting point for thin ice.⁶⁶ Wu et al. discovered an interesting V-shaped water-ILs dynamic time-dependent interaction mechanism with the inflection point around 913 s.⁶² Furthermore, another advantage of PCM2D-COS over G-2D-COS is their convenience for seeking a blue shift or red shift of some specific IR absorption peaks.⁶⁰

Here, cellulose, chitin, and chitosan (Scheme 1) are used as the reprehensive biopolymers and [EMIM][Ac] (Scheme 1) as the representative AcILs. The atmospheric water environment is achieved by exposing pure [EMIM][Ac] and mixtures of [EMIM][Ac] with biopolymers directly to moist air via an ATR-IR instrument *in situ*. We measured the hygroscopicity and ATR-IR of the above systems. Then, deconvolution, derivative, difference, and 2D-COS (including s-G-2D-COS, as-G-2D-COS, s-PCM2D-COS, and as-PCM2D-COS) IR techniques were used to analyze the ATR-IR spectra. For a better interpretation of the hygroscopicity observation and *in situ* 2D-COS ATR-IR spectroscopy, a hypothetic dynamic mechanism was proposed to explain the three-regime pattern of these systems. The dynamic atmospheric water sorption in [EMIM][Ac] and [BMIM][Ac] was investigated by the Mulliken charge distribution, IR shift of peak position, and 2D-COS. Finally, a more subtle analysis on the chemisorption and physisorption of CO_2 was conducted to verify the presumption of CO_2 capture from the air by these systems.

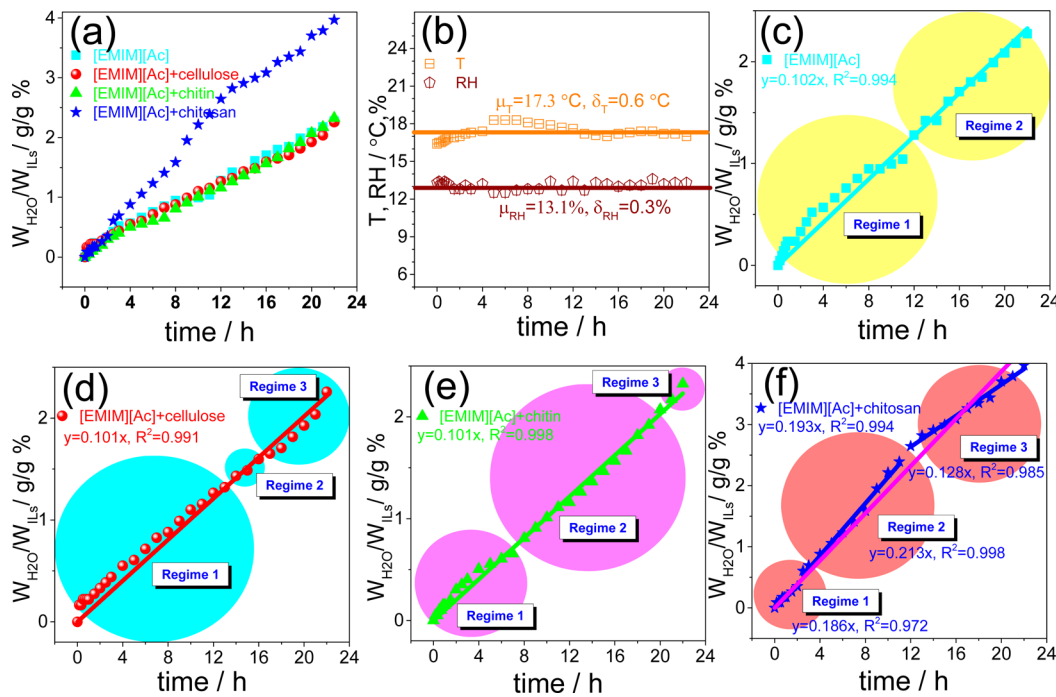


Figure 1. Hygroscopicity, temperature (T), and relative humidity (RH) as a function of time within 22 h for pure [EMIM][Ac] and its mixtures with biopolymers exposed to moist air. Overall presentation of hygroscopicity (a), data of T and RH (b), specific hygroscopicity of pure [EMIM][Ac] (c), and its mixtures with cellulose (d), chitin (e), and chitosan (f).

2. EXPERIMENTAL SECTION

2.1. Materials. [EMIM][Ac] with a purity of more than 99% was obtained from Lanzhou Greenchem ILs, LICP, CAS (Lanzhou, China). N₂ (99.999%) and CO₂ (99.995%) were supplied by Beijing Huayuan Gas Chemical Industry Co., Ltd. (Beijing, China). Cellulose was purchased from Sigma-Aldrich (St. Louis, USA). Chitosan was purchased from Sinopharm Chem. Reagent Co. Ltd., having an 80.0–95.0% deacetylation degree. The cellulose, chitin, and chitosan samples were dried at 150 °C for about 12 h under a vacuum before dissolving in [EMIM][Ac]. Similarly, the [EMIM][Ac] sample was also loaded onto the vial and then placed in a vacuum oven at 60 °C for 80 h before use, with some P₂O₅ placed onto another vial nearby for a better desiccant. The impurities of [EMIM][Ac] include water (less than 850 ppm measured by Karl Fisher titration) and halogen ion (undetectable by AgNO₃ precipitation). Other impurities were undetectable by NMR measurement (Bruker AM, 400 MHz spectrometer). No detectable change of NMR spectra and IR spectra of [EMIM][Ac] was found before and after the drying, implying a negligible thermal degradant of the [EMIM][Ac] during the drying process.

2.2. Dissolution of the Biopolymers Cellulose, Chitin, and Chitosan in [EMIM][Ac]. Three samples of dried [EMIM][Ac] (ca. 6.0 g for each) were added in three 3-neck round-bottom flasks (100 mL). Then, these flasks were immersed in an oil bath (DF-101S, Henan Yuhua Instrument Factory, with temperature instability of about ± 1.0 °C). Finely grinded cellulose, chitin, and chitosan powders (0.1 wt % of the IL for every time) were added into these flasks, respectively, where the oil was continuously stirred and was purged with N₂ as the protective gas. The starting temperature of the oil bath was set as 40 °C, and then was increased to a constant temperature of 100 °C. Additional cellulose, chitin, and chitosan powders (another 0.1 wt % of the IL) were added

into [EMIM][Ac] repeatedly until their mass fraction reached 4%.

2.3. ATR-IR Spectra Measurement. The couple of the attenuated total reflection (ATR-IR) equipment with the FTIR spectrometer (Prestige-21, Shimadzu, Japan, DTGS detector) was used. We prepared the samples before the experiment. Then, one of two drops of dried samples (i.e., pure [EMIM][Ac] and its mixtures with cellulose, chitin, and chitosan) were placed on the ATR Cell (ATR-8200H, made of ZnSe, 584 mm² surfaces, 45° incident angles). It meant that these samples were directly exposed to moist air. After the sample load, this sample was scanned (with the speed of every 10 min until 360 min), during which the samples were not stirred or mixed. The intensity and positions of all peaks were found to be a negligible change after 360 min; at this time, we would stop the ATR-IR measurement. Meanwhile, a temperature and humidity sensor (which would be discussed in section 2.4 as well) was placed nearby to record the data of room temperature and relative humidity (17 °C, 13% on average, respectively). Resolutions, scans, and wavenumber spans of all the samples for ATR-IR investigated were set as 4, 40, and 4200 cm⁻¹ (ranging from 4600 to 400 cm⁻¹), respectively.

2.4. Moisture Sorption Measurement. The atmospheric water sorption in these systems was measured in a weighing room with the sample exposed to the air for 22 h straight. Four glass bottles (5 mL) were first placed on four analytic balances (± 0.1 mg, Adventure AR224CN, Ohaus). Then, pure [EMIM][Ac] and mixtures of [EMIM][Ac] with biopolymers (ca. 0.5 g for each sample) were placed onto the bottom of four glass bottles, respectively. For a better uniform distribution, we also stirred the convex sample into the concave place via a dropper. Meanwhile, a temperature (T) and relative humidity (RH) sensor (Testo 608-H2, Germany, ± 0.2 °C T , $\pm 2\%$ RH) was put nearby to detect the temperature and relative humidity data. The data of mass, temperature, and

relative humidity as a function of time are given in Figure 1. The experimental process was similar to our previous reports.^{67,68} The mass gain could thus be all attributed to water absorbed from moist air, because the gas (N_2 , O_2 , and CO_2) solubility in the ILs could be neglected due to the low partial pressure of CO_2 or the low solubility of N_2 and O_2 .^{34,67,69} The average temperature and relative humidity within 22 h was $\mu_T = 17.3^\circ C$ ($\delta_T = 0.6^\circ C$) and $\mu_{RH} = 13.1\%$ ($\delta_{RH} = 0.3\%$), respectively (Figure 1), where μ and δ indicate the mean value and standard deviation, respectively. The temperature and relative humidity can be assumed as constant in the process of hygroscopicity measurement. The unit for the amount of atmospheric water sorption in $[EMIM][Ac]$ (W_{H_2O}) was the mass ratio of water to ILs, i.e., g/g H_2O/ILs .

2.5. G-2D-COS, auto-MW2D-COS, and PCMW2D-COS. All 2D-COS (including s-G-2D-COS, as-G-2D-COS, s-PCMW2D-COS, and as-PCMW2D-COS) were processed by using the conventional 2D *shige* software (<http://sci-tech.ksc.kwansei.ac.jp/~ozaki/2D-shige.htm>), which has been extensively applied for investigating the dynamic process and seeking subtle information from the overlapped peaks.^{62,63,70} The window size ($2m + 1$) was selected as 11 for all of the 2D-COS calculations. Further plot-drawing with the data derived from 2D *shige* was conducted by Origin Professional 9.0, by which the planar and stereoscopic figures could be better illustrated.

3. RESULTS AND DISCUSSION

3.1. Assignment of IR Spectroscopy. The overview of schemes (Schemes 1–3 and Schemes S1 and S2, Supporting Information) and figures (Figures 1–6 and Figures S1–S4, Supporting Information) and the assignment of the IR spectroscopy are introduced in section S0 of the Supporting Information. Particular attention is the hygroscopicity data analysis (Figure 1), s-PCMW2D-COS (Figure 2), and as-PCMW2D-COS (Figure 3) ATR-IR spectra.

3.2. Hygroscopicity of $[EMIM][Ac]$ and Mixtures of $[EMIM][Ac]$ with Biopolymers. Figure 1 shows that the mixture of $[EMIM][Ac]$ with chitosan has a much greater hygroscopicity capacity (ca. 2 times) and rate (ca. 1.8, 2, 1.3, and 1.9 times in regime 1, regime 2, regime 3, and the overall fitted curve, respectively) than those of the other three systems (Figure 1a), which are almost identical at the experimental conditions (Figure 1b). We also find that moisture uptake shows a clear three-regime tendency for the mixture of $[EMIM][Ac]$ with chitosan (Figure 1f, 0–2 h for regime 1, 2.5–12 h for regime 2, and 12–22 h for regime 3), a less clear three-regime situation for the mixture of $[EMIM][Ac]$ with chitin (Figure 1e, 0–7 h for regime 1, 8–20 h for regime 2, and 21–22 h for a very short and unclear regime 3), the least clear three-regime division for the mixture of $[EMIM][Ac]$ with cellulose (Figure 1d, 0–13 h for regime 1, 14–16 h for a very short and unclear regime 2, and 17–22 h for regime 3), and a two-regime zone for pure $[EMIM][Ac]$ (Figure 1c, 0–11 h for regime 1 and 12–22 h for regime 2).

The division of the regimes for the hygroscopicity of the mixture of $[EMIM][Ac]$ with chitosan could be directly visualized from Figure 1f. The fitted slopes of regime 1 (0.186), regime 2 (0.213), regime 3 (0.128), and the overall fitted slope (0.193) of the mixture of $[EMIM][Ac]$ with chitosan are higher (ca. 1.8, 2, and 1.3 times consecutively and 1.9 times for the overall fitted slope) than other systems (ca. 0.101 for the three categories).

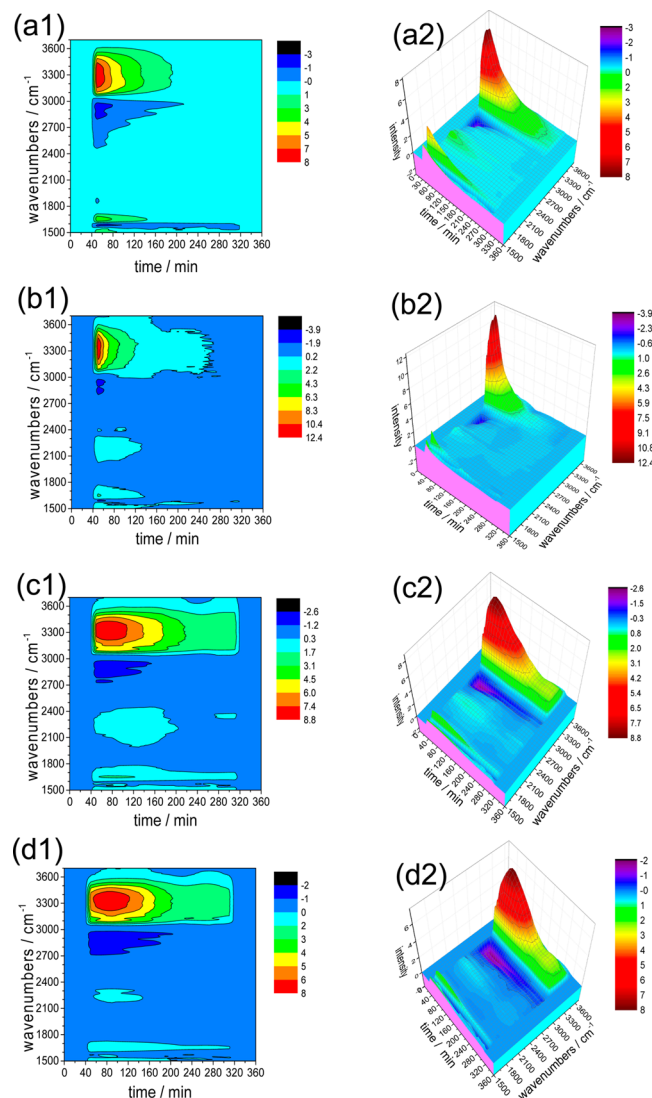


Figure 2. Planar (1) and stereoscopic (2) s-PCMW2D-COS ATR-IR spectra of pure $[EMIM][Ac]$ (a) and its mixtures with cellulose (b), chitin (c), and chitosan (d) absorbing atmospheric water.

The mixtures of $[EMIM][Ac]$ with chitin (Figure 1e) and cellulose (Figure 1d) have similar three-regime-mode divisions. Both of them have an overlapping slope between regime 2 and the overall regression and a greater change rate of regime 1 than the overall fitted curve. However, the overlapping time period between regime 2 and the overall regression for the mixture of $[EMIM][Ac]$ with chitin (12 h) is much longer than that for the mixture of $[EMIM][Ac]$ with cellulose (2 h). If we conceive that regime 2 of the mixture of $[EMIM][Ac]$ with chitosan also belongs to this overlapping region, the overlapping time for the mixture of $[EMIM][Ac]$ with chitosan (9.5 h) will be comparable to that for the mixture of $[EMIM][Ac]$ with chitin. Thus, the change rate of each regime of the mixture of $[EMIM][Ac]$ with chitin is greater, comparable, and greater than that of the overall fitted curve, while the mixture of $[EMIM][Ac]$ with cellulose has a greater, comparable, and less change rate than that of the overall fitted curve.

For pure $[EMIM][Ac]$, regime 2 is totally overlapped with the overall fitted curve; hence, only two regimes occur (Figure 1c). Pure $[EMIM][Ac]$ and mixtures of $[EMIM][Ac]$ with cellulose and chitin have a greater slope of regime 1 than the

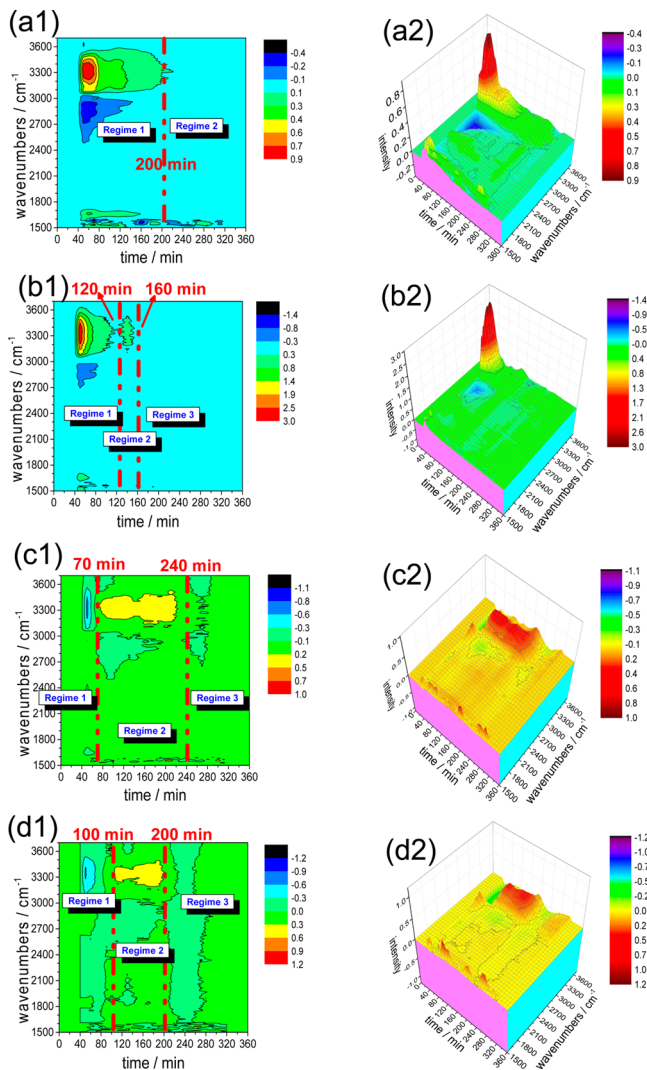


Figure 3. Planar (1) and stereoscopic (2) as-PCM2D-COS ATR-IR spectra of pure [EMIM][Ac] (a) and its mixtures with cellulose (b), chitin (c), and chitosan (d) absorbing atmospheric water.

overall fitted line (Figure 1c), with the first regime having a more robust water sorption rate. The above three systems all have a robust initial water sorption rate in regime 1, followed by a slower water sorption rate in regime 2. They are different in regime 3: convergence with regime 2 or not existence, lower rate than regime 2 or overall fitted curve, and greater rate than regime 2 or overall fitted curve, respectively.

Why do such obvious differences exist among the hygroscopicities of these systems? Why is the hygroscopicity of the mixture of [EMIM][Ac] with chitosan abnormally (ca. 2 times) greater than those of the other systems? Why is the three-regime atmospheric water sorption process in the mixture of [EMIM][Ac] with chitosan so clear, while it is less clear (a very short and unclear regime 3) in the mixture of [EMIM][Ac] with chitin and the least clear (a very short and unclear regime 2) in the mixture of [EMIM][Ac] with cellulose? Why does the pure [EMIM][Ac] have a two-regime hygroscopicity mode rather than a three-regime pattern? These phenomena are not caused by the deviation of temperature and relative humidity because the highest hygroscopicity and the clearer three-step atmospheric water sorption mechanism only occur in the mixture of [EMIM][Ac] with chitosan. The same

conclusion is drawn from the data of 2D-COS IR and the hygroscopicity observation, which would be discussed later.

3.3. 2D-COS IR of Pure [EMIM][Ac] and the Mixtures of [EMIM][Ac] with Biopolymers. Besides the macroscopic hygroscopicity experiment, in situ microscopic ATR-IR spectroscopy of the four systems by exposing thin layer samples to moist air for a time period was carried out, and then analyzed by using the 2D-COS technique to corroborate the regime-dividing envisage. The 2D-COS technique could be used to interpret hidden or overlapped peaks, and discriminate the dividing points of the dynamic process.⁶⁰ A much shorter saturated time (ca. 6 h) occurs for the ATR-IR measurement than the hygroscopicity survey (more than 22 h), since the sample on the ATR cell is thinner than that in the hygroscopicity experiment. The penetration length of ATR-IR might also reduce the time necessary to reach the change limit of peak intensity. However, it does not affect our intention to apply the fast-changing microscopic ATR-IR experiment (particularly after being processed with the as-PCM2D-COS technique) to demonstrate the slow-changing macroscopic hygroscopicity observation related to regime division.

Parts a1 and a2 of Figure 3 show the as-PCM2D-COS IR spectroscopy of atmospheric water sorption in pure [EMIM][Ac] by using the spectral variable (i.e., wavenumber) and perturbation variable (i.e., time) as the vertical and horizontal axes, respectively. A drastic change is found at ca. 200 min in as-PCM2D-COS around 3300 cm⁻¹ for the OH stretching vibration peak of atmospheric water (Figure 3a1 and a2). It indicates the existence of a drastic intensity change rate before 200 min but a slow change after 200 min, according to Morita's rule for the interpretation of as-PCM2D-COS.⁶⁰ Namely, the atmospheric water sorption in pure [EMIM][Ac] could be divided into two regimes: regime 1 (before 200 min) and regime 2 (after 200 min). It is consistent with the hygroscopicity data discussed above, during which the water sorption rate of regime 1 is greater than the overall change rate while the change rate of regime 2 is lower than that (Figure 1c). The greater water sorption rate in regime 1 than that in regime 2 could be observed in both microscopic ATR-IR and macroscopic hygroscopicity measurements. The two regimes-time-dividing points by hygroscopicity observation and microscopic in situ 2D-COS ATR-IR is not in coincidence due to a faster saturated water sorption in the ATR-IR experiment caused by the thinner sample than that in the hygroscopicity observation, and by the existence of a penetration length limit, or absorbance limit.

The water sorption in the mixture of [EMIM][Ac] with cellulose has three regimes but with an indiscernible regime 2 according to hygroscopicity data analysis (Figure 1d). Unexpectedly, we also find the same characteristics of three regimes accompanied by a vague regime 2 in the corresponding as-PCM2D-COS IR spectroscopy in terms of OH stretching vibration around 3300 cm⁻¹ (Figure 3b1 and b2). The as-PCM2D-COS IR spectroscopy of the [EMIM][Ac]/water system shows two dividing points at 120 and 160 min, i.e., regime 1 before 120 min, regime 2 between 120 and 160 min, and regime 3 after 160 min (Figure 3b1 and b2). The time scale of regime 2 is much less than those of regime 1 and regime 3 (Figure 3b1 and b2), resembling the conclusion drawn from hygroscopicity data (Figure 1d). The sorption rate in regime 1 is greater but becomes slower in regime 3, also coinciding with the hygroscopicity observation. Obviously, the microscopic

regime divisions from as-PCM2D-COS are more distinct than those from hygroscopicity data.

The mixtures of [EMIM][Ac] with cellulose and chitin show a short and unclear regime 3 rather than regime 2 as discussed above. The as-PCM2D-COS IR spectroscopy of the mixture of [EMIM][Ac] with chitin also corroborates this feature. Parts c1 and c2 of Figure 3 show two inflection points at ca. 70 and 240 min around the OH stretching band at ca. 3300 cm^{-1} from as-PCM2D-COS. Thus, a three-regime water sorption process in the mixture of [EMIM][Ac] with chitin could be concluded. The time scale for regime 3 from as-PCM2D-COS in Figure 3c1 and c2 seems very short, not ranging from 240 to 360 min as expected. Obviously, the microscopic regime divisions from as-PCM2D-COS are more distinct than those from hygroscopicity data. One of the discrepancies between as-PCM2D-COS and hygroscopicity observation is that water sorption in regime 2 derived from as-PCM2D-COS is the highest in the three regimes, while that derived from hygroscopicity data is medium. It might be due to the differences in sample thickness and surface area exposed to the moist air. In spite of this discrepancy, both the macroscopic and microscopic measurements show a three-regime tendency, which is actually our main focus. Further discussion would be described as below.

The as-PCM2D-COS IR spectra (Figure 3c1, c2, d1, and d2) of mixtures of [EMIM][Ac] with chitosan and chitin are similar because chitin and chitosan have similar structures (Scheme 1). Three regimes exist (regime 1 before 100 min, regime 2 between 100 and 200 min, and regime 3 after 200 min), in which regime 2 has the greatest OH intensity changing rate than the other two regimes. The main difference in as-PCM2D-COS is that the time scale of regime 3 along the OH stretching vibration is very short and indiscernible for the mixture of [EMIM][Ac] with chitin (Figure 3c1 and c2), while it is very clear for the mixture of [EMIM][Ac] with chitosan (Figure 3d1 and d2). This phenomenon might be caused by the difference in the content of NH_2 in chitin and chitosan. The microscopic as-PCM2D-COS (Figure 3d1 and d2) and macroscopic hygroscopicity measurement (Figure 1f) for the mixture of [EMIM][Ac] with chitosan are consistent, since the water sorption rate increases in regime 2 and then decreases in regime 3.

By combining the macroscopic hygroscopicity measurement and microscopic ATR-IR experiment, we can obtain the following conclusions: the mixture of [EMIM][Ac] with chitosan has a clear three-regime zone with a lower, greater, and then lower water sorption rate; the mixture of [EMIM][Ac] with chitin has indiscernible three-regime partitions in regime 3 with a greater, lower, and then greater moisture sorption rate; the mixture of [EMIM][Ac] with cellulose has indiscernible three-regime compartments in regime 2 with a greater, moderate, and then lower humidity uptake rate; pure [EMIM][Ac] has clear two-regime divisions with a greater and then lower water sorption rate. Here we would interpret these characteristic data related to hygroscopicity measurement and ATR-IR observation. The shift in peak position for these systems in Figure S4 (Supporting Information) would provide additional evidence for our proposed mechanisms.

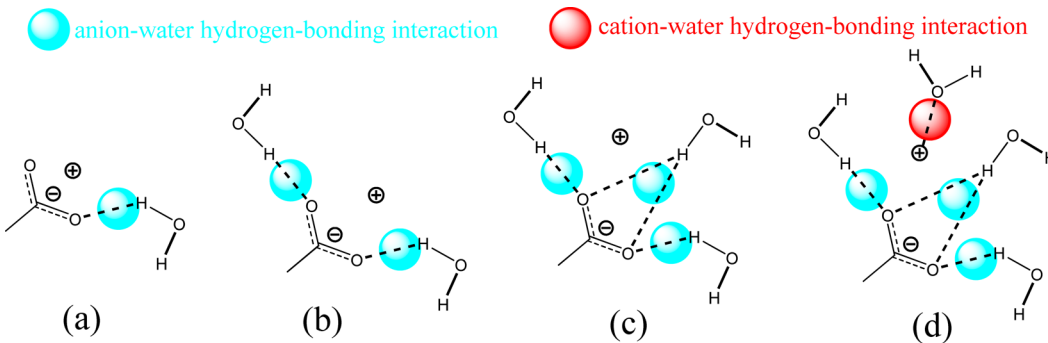
3.4. Proposed Hypothetic Dynamic Mechanism to Explain Hygroscopicity Differences among the Discussed Systems. Some discussions in this part are based on some basic knowledge, and they are given in the Supporting Information (section S1). Before explaining the difference in

hygroscopicity for pure [EMIM][Ac] and its mixtures with biomass, five assumptions and validities are raised (section S1, Supporting Information). In a word, these assumptions for exclusively explaining hygroscopicity differences among pure [EMIM][Ac] and its mixtures with biomass include the following: there exists strong anion–cation hydrogen bonds in [EMIM][Ac] (assumption 1); dissolution of biomass in [EMIM][Ac] mainly involves anion–biomass hydrogen bonds, leading to the production of a freer cation than that in pure [EMIM][Ac] (assumption 2); no biomass precipitation would occur after atmospheric water interacts with only the bulk [EMIM][Ac] via mainly water–anion hydrogen bonds, while the proportion of water–cation in biomass/[EMIM][Ac] mixtures would be higher than that in pure [EMIM][Ac] due to their freer cation (assumption 3); chitosan (other than cellulose, chitin, or pure IL), after dissolved by [EMIM][Ac], would produce an obvious free NH_2 group (assumption 4); and the atmospheric CO_2 solubility in pure [EMIM][Ac] and its mixtures with biomass is negligible when compared to the atmospheric water absorption (assumption 5). Details for these assumptions and the corresponding validities could be seen in the Supporting Information (section S1).

We take the mixture of [EMIM][Ac] with chitosan as an example to illustrate the dynamic process of atmospheric water sorption with additional evidence from the peak position shift in Figure S4 (Supporting Information).

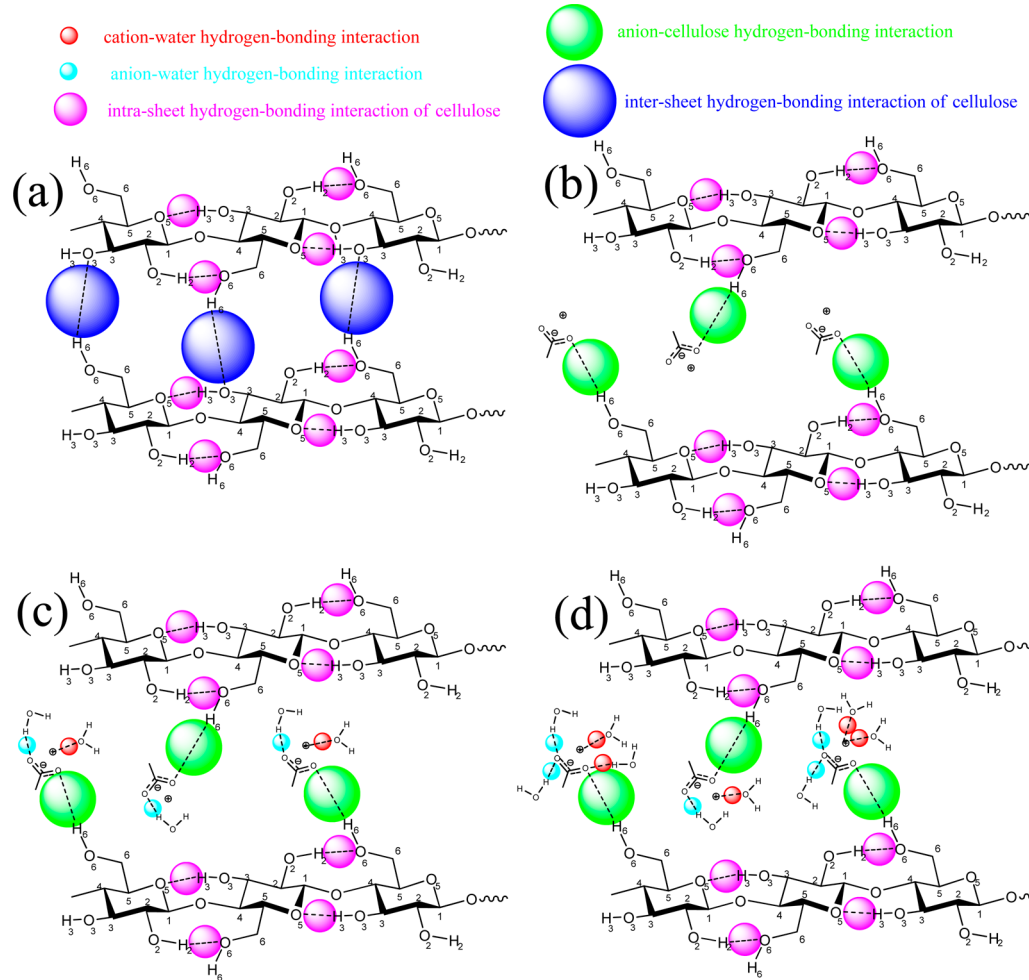
There are many intersheet (mainly $\text{O}_6\text{H}_6\cdots\text{O}_6\text{H}_6$) and intrasheet hydrogen bonds (mainly $\text{O}_3\text{H}_3\cdots\text{O}_5\text{H}_5$ and $\text{NH}_2\cdots\text{O}_6\text{H}_6$) in chitosan (Scheme S2a, Supporting Information). The $\text{O}_6\text{H}_6\cdots\text{O}_6\text{H}_6$ and $\text{NH}_2\cdots\text{O}_6\text{H}_6$ hydrogen bonds are weaker than $\text{O}_3\text{H}_3\cdots\text{O}_5\text{H}_5$ hydrogen bonds.⁷⁰ Thus, the dissolution of chitosan in [EMIM][Ac] mainly involves the break of $\text{O}_6\text{H}_6\cdots\text{O}_6\text{H}_6$ hydrogen bonds and $\text{NH}_2\cdots\text{O}_6\text{H}_6$ hydrogen bonds by forming new $\text{O}_6\text{H}_6\cdots\text{anion}$ hydrogen bonds. Because the chitosan mainly interacts with the anion of [EMIM][Ac], after the chitosan dissolution, the NH_2 and cation are freed from $\text{NH}_2\cdots\text{O}_6\text{H}_6$ and cation–anion hydrogen bonds (Scheme S2b, Supporting Information), leading to the production of a freer cation than that in pure [EMIM][Ac] and chitosan (other than cellulose, chitin). Since no chitosan precipitation occurs after atmospheric water sorption, when the mixture of [EMIM][Ac] with chitosan is exposed to moist air, the absorbed water first interacts mainly with the anion (water–anion) and the free cation (water–cation) but slightly with the free NH_2 (water– NH_2) (regime 1, Scheme S2c, Supporting Information) by hydrogen-bonding interaction (S1). Then, the absorbed water begins to form stronger and more hydrogen-bonding interactions with the free NH_2 (water– NH_2), during which the hydrogen bonds of water–anion and water–cation in regime 1 also exist (regime 2, Scheme S2d, Supporting Information). Owing to more and stronger water– NH_2 hydrogen bonds, the water sorption in this regime (0.213) is greater than that in the first regime in spite of a decreasingly weaker strength of water–anion and water–cation than regime 1 (0.186). Finally, only little formation of water– NH_2 hydrogen bonds exists in this stage, and the water is mainly absorbed via water–anion and water–cation hydrogen bonds (regime 3, Scheme S2e, Supporting Information). The strength of hydrogen bonds for water–anion and water–cation in regime 3 is weaker than that in regime 1 and regime 2, which results in the slowest sorption rate in regime 3 (0.128).

Scheme 2. Proposed Atmospheric Water Sorption Process in Pure [EMIM][Ac]^a



^aStructure of [EMIM][Ac] (a), solvation of the anion of [EMIM][Ac] by water (b), more solvation of the anion of [EMIM][Ac] by water (c), and solvation of the produced free cation of [EMIM][Ac] by water (d).

Scheme 3. Proposed Atmospheric Water Sorption Process in the Mixture of [EMIM][Ac] with Cellulose^a



^aStructure of cellulose (a), dissolution of cellulose by [EMIM][Ac] (b), water sorption in the mixture of [EMIM][Ac] with cellulose through anion/water and free cation/water hydrogen-bonding interaction (c), and more but strength-decreasing anion/water and free cation/water hydrogen-bonding interaction (d).

Chitin has a higher content of NHCOCH₃ due to a large degree of acetylation, while chitosan possesses a higher content of NH₂. C=O of the chitin forms stronger intersheet (C=O...HNCOCH₃) and intrasheet (C=O...H₂O₆) hydrogen bonds (Scheme S1a, Supporting Information) than NH₂ in chitosan (intrasheet H₂N...H₂O₆) except similar strong intrasheet O3H₃...OSHS and weak intersheet O6H₆...O6H₆ hydrogen

bonds; hence, the chitin is more stable and harder to be dissolved in ILs (e.g., [EMIM][Ac]) than chitosan.^{21,71} For a better comparison, the mole fraction of biopolymer in [EMIM][Ac] is controlled to ca. 4%. Since dissolution of biopolymer in [EMIM][Ac] mainly involves anion–biopolymer hydrogen bonds, [EMIM][Ac] dissolves chitin mainly by disrupting intersheet O6H6···O6H6 hydrogen bonds due to

their weaker strength than others (e.g., C=O···HNCOCH₃, C=O···H₂O) ^{70,72} and then forming new anion···H₂O₆ hydrogen bonds (Scheme S1b, Supporting Information). In this process, nearly no free NH₂ forms; thus, the water sorption rate in the mixture of [EMIM][Ac] with chitin (slightly more than 0.101) was only controlled by water···anion hydrogen bonds. Water···cation (in the free state) hydrogen bonds are weaker than those in the mixture of [EMIM][Ac] with chitosan (0.186), which has additional water···NH₂ interaction due to the possession of more free NH₂ (Scheme S1c, Supporting Information, regime 1), leading to the production of a freer cation than that in pure [EMIM][Ac]. Since no chitin precipitation occurs after atmospheric water sorption, water only interacts with the bulk [EMIM][Ac] via mainly water···anion hydrogen bonds, similar to the analysis of chitosan. In the absence of free NH₂, the hygroscopicity rate of the mixture of [EMIM][Ac] with chitin in regimes 2 and 3 is lower than that in regime 1 which even seems like an overlapped tendency (Scheme S1d, Supporting Information, regime 2 and regime 3), unlike the more robust water sorption rate of regime 2 in the mixture of [EMIM][Ac] with chitosan due to the overriding water···NH₂ hydrogen bonds.

Nevertheless, mainly the anion–water hydrogen bonds (Scheme 2b, regime 1) exist in atmospheric water sorption in pure [EMIM][Ac] (Scheme 2a). As time elapses (i.e., more atmospheric water is absorbed), some aggregation of water around the anion might form (Scheme 2c, regime 2). After the anion of [EMIM][Ac] is thoroughly surrounded by water, water might form hydrogen bonds with the cation by a weaker interaction (Scheme 2d, regime 3). Note that, in the case of pure [EMIM][Ac], the content of free cation is the least and the time to form a hydrogen bond with a free cation is the latest due to the strongest constraint from the anion compared to the mixtures of [EMIM][Ac] with biopolymer, thus also leading to the convergence of regime 2 and regime 3 into one regime (i.e., regime 2, as shown in Scheme 2c and d). The water sorption rate in regime 2 would be slower due to the stronger hydrogen-bond-donating anion having been occupied with water. The IR blue shift for the anion of pure [EMIM][Ac] is greater than those of the other three remaining species (Figure S4, Supporting Information). It is probably because most of the acetate anions were occupied by the biopolymer, and thus less anions were left to be hydrogen-bonded with water, leading to a lesser red shift of anion in the investigated systems after the atmospheric water perturbation. However, the blue shift of C2H for the pure [EMIM][Ac] is less than those for mixtures of [EMIM][Ac] with cellulose, chitin, and chitosan before and after water introduction (Figure S4, Supporting Information), which might be due to the freer cation in mixtures than in pure [EMIM][Ac].

As to the evolutional hygroscopicity of the mixture of [EMIM][Ac] with cellulose, the intrasheet O₆H₆···O₃H₃ hydrogen bonds are easier to break than the intersheet O₃H₃···O₅H₅ and O₂H₂···O₆H₆ hydrogen bonds in cellulose (Scheme 3a). When cellulose (4% mol. fra.) is dissolved in [EMIM][Ac], mainly the more vulnerable intrasheet hydrogen bonds (i.e., O₆H₆···O₃H₃) are disrupted due to the stronger O₆H₆···anion hydrogen-bonding interaction (Scheme 3b). Meanwhile, some cations would be freed after the fixation of anion by the hydroxyl of cellulose (Scheme 3b). When we expose the mixture of [EMIM][Ac] with cellulose to atmospheric water, the water would be tethered to the anion first because of the greater hydrogen-bonding ability between

the hydrogen-bonding donor of the acetate anion and the acceptor of water (Scheme 3c, regime 1). Also, in this step, a weak hydrogen-bonding interaction between the water and free cation would be formed (Scheme 3c, regime 1), which compensates for the hygroscopicity reduced by fixation of the anion compared to pure [EMIM][Ac], thus forming a comparative hygroscopicity between pure [EMIM][Ac] and the mixture of [EMIM][Ac] with cellulose. The change of the subsequent regime would be negligible, thus emerging an indiscernible regime 2 and regime 3, as shown in Scheme 3d.

The interactions of water with the investigated systems could be divided into three components: water–anion, water–free cation, and water–biopolymer. Restrained water–anion interaction and enhanced water–free cation interaction for pure and the mixture of [EMIM][Ac] with biopolymer are almost the same. For instance, cellulose/[EMIM][Ac] has a weaker anion···water hydrogen-bonding interaction in Scheme 3b (due to the stronger anion–cellulose interaction caused by weaker intersheet O₆H₆···O₃H₃ and intrasheet O₃H₃···O₅H₅ and O₂H₂···O₆H₆ hydrogen bonds, as shown in Scheme 3a, supported by the greater saturated solubility) than those in chitin/[EMIM][Ac] and chitosan/[EMIM][Ac], which is compensated by the freer cation (stronger anion···cellulose interaction means weaker anion···cation interaction, hence a freer cation in the mixture of [EMIM][Ac] with cellulose) that is hydrogen-bonded with water (Scheme 3c, regime 1). In this way, the overall affinity of atmospheric water to cation and anion for the investigated systems would be similar. Similar to the mixture of [EMIM][Ac] with chitin, the mixture of [EMIM][Ac] with cellulose in regime 2 and regime 3 (Scheme 3d) shows a lower water sorption rate and an indiscernible partition.

The biopolymers in [EMIM][Ac] have different effects on the hygroscopicity, although their contents only reach 4% mole fraction. Unexpectedly, the hygroscopicity of the mixture of [EMIM][Ac] with cellulose (0.101) and with chitin (0.101) is negligible, which is also similar to that of pure [EMIM][Ac] (0.102). However, the hygroscopicity of the mixture of [EMIM][Ac] with chitosan is double those of the other three systems; thus, the effect of chitosan could not be ignored. The most possible reason is the presence of the NH₂ group in chitosan freed from the disruption of intrasheet H₂N···H₂O₆ by [EMIM][Ac] after dissolution, leading to additional hygroscopicity. No such additional hygroscopicity effect exists in chitin (negligible NH₂ group), cellulose, and pure [EMIM][Ac] for the absence of the NH₂ group. Interestingly, the double effect here is similar to the double effect of CO₂ sorption capacity in the mixture of [BMIM][Cl] with chitosan than that in the mixture of [BMIM][Cl] with chitin.⁷¹

The existence of a free NH₂ group produced from the mixture of [EMIM][Ac] with chitosan could also be derived from the dissolution data of chitin and chitosan in [EMIM][Ac]. Note that, in Schemes S1 and S2 (Supporting Information), we assume that the chitin only contains a NHCOCH₃ group (Scheme S1, Supporting Information) and chitosan only contains a NH₂ group (Scheme S2, Supporting Information). As a matter of fact, there is also NH₂ existing in chitin and NHCOCH₃ existing in chitosan, but the contents of NH₂ in chitin and of CH₃CONH₂ in chitosan are much less than those of the NHCOCH₃ in chitin and NH₂ in chitosan, respectively. A higher saturated solubility of chitosan in [EMIM][Ac] (ca. 12 wt. fra.^{%21}) than chitin in [EMIM][Ac] (ca. 6 wt. fra.^{%21}) indicates a higher possibility of NH₂···O₂H₂

hydrogen bond disruption in chitosan than C=O···H₂O2 hydrogen bond disruption in chitin. Thus, the easier disruption of NH₂···O2H2 hydrogen bonds in chitosan when chitosan is dissolved in [EMIM][Ac] would favor the release of a free NH₂ group, which could be a good CO₂ absorbent⁷¹ or hygroscopic agent.

3.5. CO₂ Capture during the Atmospheric Water Sorption Process by Pure [EMIM][Ac] and Mixtures of [EMIM][Ac] with Biopolymer. In the above discussion, the mass gain of the investigated systems exposed to the air is all attributed to the sorption of atmospheric H₂O other than atmospheric gases (e.g., O₂, N₂, and CO₂) absorption. The partial pressure of CO₂ in the atmosphere is ca. 40 Pa. It is well-known that CO₂ could be physically dissolved^{7,73} in conventional ILs or chemically reacted^{4,8,16,74–79} with functionalized ILs, rendering the possibility of CO₂ capture by ILs. An interesting thing reported by many researchers is that the AcILs,^{50,51,80–83} such as [EMIM][Ac] and [BMIM][Ac], could form a chemically stable complex with CO₂. Our previous study also showed that the CO₂ solubility in [BMIM][Ac] is abnormally greater than that in other conventional ILs (e.g., [BMIM][BF₄] and [BMIM][PF₆]).⁸³

A previous study reported that a dinuclear copper(I) complex could be oxidized in air by CO₂ rather than O₂,⁸⁴ which gave us a cue to test whether [EMIM][Ac] could absorb CO₂ from the atmosphere. Actually, other materials,^{52–55,85–89} such as amine-tethered solid absorbent and sodium hydroxide spray, have shown a favorable efficiency to capture CO₂ from the air. Most studies (including our previous investigations) ignored the atmospheric CO₂ capture by ILs when exploring the hygroscopicity.^{27–29,31,33,34,67–69,90} Since AcILs could react with CO₂, CO₂ might exist in AcILs after being exposed to air for a long term. Therefore, we assume that [EMIM][Ac] could absorb a trace of CO₂ from the air due to the unusual high CO₂ solubility in spite of their high hygroscopicity^{5,34} and the hindrance of the CO₂ absorption⁴⁷ by the hygroscopicity. During the atmospheric water sorption process in these investigated systems by *in situ* ATR-IR, we found the existence of a CO₂ IR peak with both physisorption and chemisorption.

The physisorption of atmospheric CO₂ in pure [EMIM][Ac] and mixtures of [EMIM][Ac] with biopolymers could be seen by the IR peak blue shift from ca. 2330 to ca. 2350 cm⁻¹ with time (Figures S1a1 and a2, Supporting Information). The intensity increase of the 2335 cm⁻¹ peak could also be seen in the s-G-2D-COS (Figure S2a1, Supporting Information). Blath et al.⁹¹ also witnessed a new IR peak around 2345 cm⁻¹ after treatment of [EMIM][Ac] by CO₂ and assigned this peak to the dissolved CO₂. We observe a new peak around 2345 cm⁻¹ in the [EMIM][Ac]/CO₂ solution, as shown in Figure 5a and b. The blue shift of atmospheric CO₂ in [EMIM][Ac] could be interpreted as follows: CO₂/[EMIM][Ac] interaction is stronger once CO₂ contacts with [EMIM][Ac], leading to a lower peak position at the beginning. As time elapses, CO₂/[EMIM][Ac] interaction decreases, resulting in a relatively higher CO₂ IR peak position.

Besides pure [EMIM][Ac], mixtures of [EMIM][Ac] with biopolymers also show this new peak shifting from ca. 2330 to ca. 2350 cm⁻¹ (Figure S1b1, b2, c1, c2, d1, and d2, Supporting Information), corresponding to the physisorption of CO₂. Similar to that of pure [EMIM][Ac], the corresponding intensity change in s-G-2D-COS also occurs (Figure S2b1, c1, and d1, Supporting Information), corroborating the CO₂ physisorption. Particularly, there is an obvious signal response

in s-PCM2D-COS for physically absorbed CO₂ at ca. 2345 cm⁻¹ in mixtures of [EMIM][Ac] with biopolymers (Figure 2b1, b2, c1, c2, d1, and d2) while not in pure [EMIM][Ac] (Figure 2a1 and a2). It might be due to the greater physical CO₂ capacity in the mixtures of IL with biopolymers than that in pure IL after the introduction of OH from cellulose or NH₂ from chitin,⁷¹ chitosan.⁷¹ Specifically, the value of the mixture of [EMIM][Ac] with chitosan (ca. 2, Figure 2d1 and d2) in s-PCM2D-COS for physical CO₂ sorption is slightly greater than that of the mixture of [EMIM][Ac] with chitin (ca. 1.7, Figure 2c1 and c2), which is consistent with Xie's report.⁷¹ As to the IR wavenumber interval ranging from ca. 2330 to ca. 2350 cm⁻¹ related to CO₂ physisorption in as-G-2D-COS, no detectable signal responds to pure [EMIM][Ac] (Figure S2a2, Supporting Information) and the mixture of [EMIM][Ac] with cellulose (Figure S2b2, Supporting Information) after being exposed to atmospheric CO₂ while the mixture of [EMIM][Ac] with chitin (Figure S2c2, Supporting Information) and the mixture of [EMIM][Ac] with chitosan (Figure S2d2, Supporting Information) have minor detection signal. It indicates a greater physically CO₂-responding ability for mixtures of IL with chitin and chitosan than pure [EMIM][Ac] and the mixture of IL with cellulose. In conclusion, the physical-CO₂-philicity of the atmosphere could be ordered as the mixture of [EMIM][Ac] with chitosan > the mixture of [EMIM][Ac] with chitin > the mixture of [EMIM][Ac] with cellulose > [EMIM][Ac].

Chemisorption of CO₂ in the investigated systems also occurs. Many reports have demonstrated the existence of CO₂ chemisorption in acetate-based ILs.^{47–51,83,91–94} Since even the nearly equimolar CO₂ sorption by amine-functionalized IL just has 3% physical CO₂ sorption at most⁷⁹ and CO₂ partial pressure in the atmosphere is so low (ca. 40 Pa), it is reasonable to deduce that CO₂ chemisorption would take up nearly all of the overall CO₂ sorption. The peak of formed carboxylate salts of the CO₂/[EMIM][Ac] chemical complex is ca. 1666 cm⁻¹, which might overlap with bending vibration of OH in atmospheric water (ca. 1650 cm⁻¹) absorbed by [EMIM][Ac]. Our IR observations also suggest the existence of such a couple (Figure S1a1, a2, b1, b2, c1, c2, d1, and d2, Supporting Information), in which CO_{2,chem} is the left shoulder and OH_b is the peak. The difference spectra in Figure S1a2, b2, c2, and d2 (Supporting Information) give a clearer couple of the two peaks. Additionally, the subshoulder peak around 1730 cm⁻¹ is also the evidence of CO₂ chemisorption. We noticed that the CO₂/[EMIM][Ac] and CO₂/[BMIM][Ac] chemical complexes showed a hidden peak around 1730 cm⁻¹ in previous reports.^{48,50,51,92} It might be due to the formation of acetate acid, which is physically dissolved in [EMIM][Ac]^{51,92,95} or hydrogen-bonded with the anion of [EMIM][Ac],^{83,96} showing the peak position around 1722 cm⁻¹. Mixtures of [EMIM][Ac] with chitin and chitosan show a split of those two bands in as-G-2D-COS (COO⁻ on the left in green color, OH_b on the right in red color) around the corresponding region when exposed to the air (Figure S2c2 and d2, Supporting Information). It clearly discriminates the couple of these two bands. Furthermore, according to Noda's rule,⁵⁶ the red-colored OH_b and green-colored COO⁻ bands suggest a more robust water perturbation than CO₂ interference; i.e., the water sorption is more remarkable than CO₂ uptake. However, this split cannot be found by exposing pure [EMIM][Ac] or the mixture of [EMIM][Ac] with cellulose to the air, which implies an increase of the ratio of CO₂ chemisorption to water sorption.

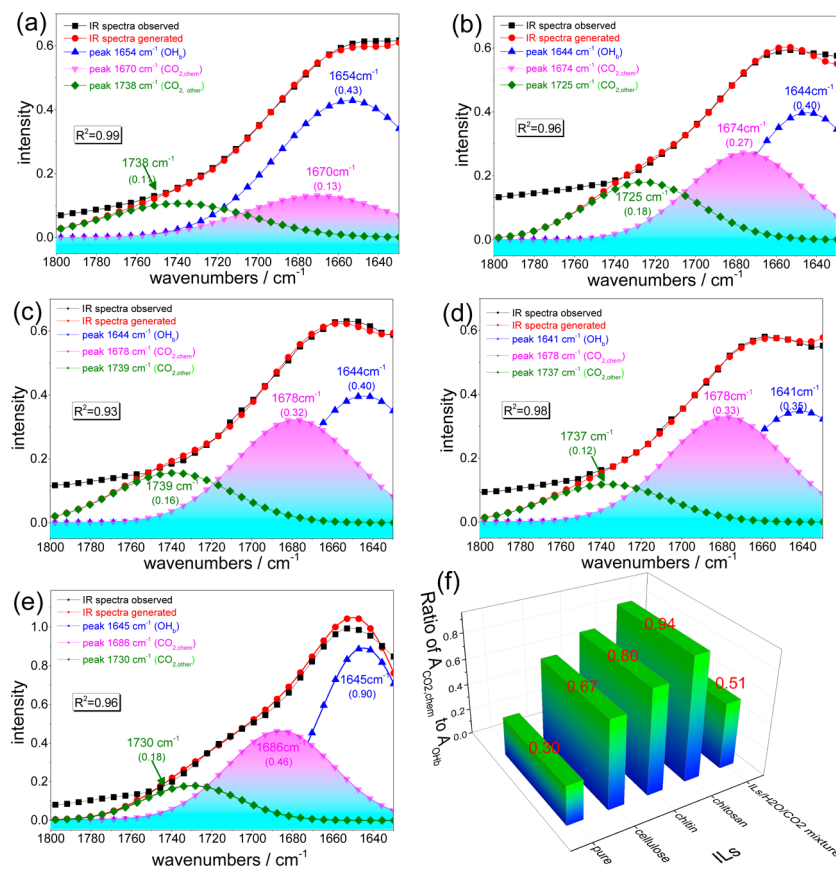


Figure 4. Deconvolution of ATR-IR coupled CO_{2,chem} and OH_b spectra ranging from ca. 1800 to 1600 cm⁻¹ for pure [EMIM][Ac] (a), and its mixtures with cellulose (b), chitin (c), and chitosan (d) to absorb atmospheric water at the end of 360 min, and for the prepared [EMIM][Ac]/CO₂/H₂O solution (e), the peak area ratio of CO_{2,chem} to H₂O for the above systems and for prepared CO₂/H₂O (f). The number in parentheses below the peak position of subset figure (a) to (e) represents the peak area of the corresponding peak. The area of peak CO_{2,chem} is filled with color for the purpose of guiding the eye.

The deconvolution of IR spectra in the corresponding range for pure [EMIM][Ac] (Figure 4a), the mixture of [EMIM][Ac] with cellulose (Figure 4b), the mixture of [EMIM][Ac] with chitin (Figure 4c), and the mixture of [EMIM][Ac] with chitosan (Figure 4d) also demonstrate this conjecture of increasing CO₂ chemisorption ratio to H₂O sorption by using their separate peak area, i.e., 0.30, 0.67, 0.80, and 0.94 (Figure 4e), respectively. Furthermore, to identify the existence of CO₂ uptake, we prepared a referred [EMIM][Ac]/H₂O/CO₂ solution (by purging 2 bar of CO₂ in 10% g/g H₂O/IL solution for about 1 h) and conducted IR measurement. IR results show a clear overlap of CO_{2,chem} (ca. 1685 cm⁻¹) with OH_b (ca. 1645 cm⁻¹, Figure 4e), corroborating the CO₂ capture from air by [EMIM][Ac] except for water sorption.

The CO₂ content in [EMIM][Ac] is also estimated by Henry's constant k_H . The CO₂ concentration in [EMIM][Ac] is approximately 0.78 (mol. fra.) % by dividing the corresponding Henry's constant (k_H = ca. 5120 Pa at 25 °C calculated by Yokozeki et al.,⁸⁰ assuming a negligible temperature difference at our experiment temperature, ca. 17 °C) by the partial pressure of atmospheric CO₂ (ca. 40 Pa). The nearly 4% mass ratio (i.e., 30% mol. fra.) water sorption from air is estimated to decrease the CO₂ solubility in [EMIM][Ac] about 55% according to interpolation from Gomes' data.⁴⁷ A nearly 50% CO₂ decrease is also witnessed in the [EMIM][Ac]/CO₂ solution when the system was exposed to the atmospheric water within 600 min (Figure 5a and b). Thus, multiplying 0.78

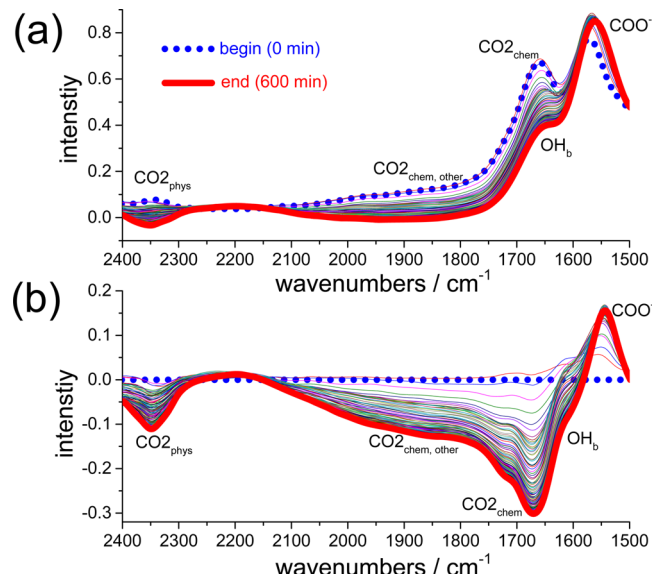


Figure 5. ATR-IR spectra of [EMIM][Ac]/CO₂ solution exposed to moist air as a function of time from 0 min (begin) to 600 min (end) with increments of 5 min with the original (a) and difference (b) formation. The reference spectrum for the difference spectra is that from the beginning at 0 min.

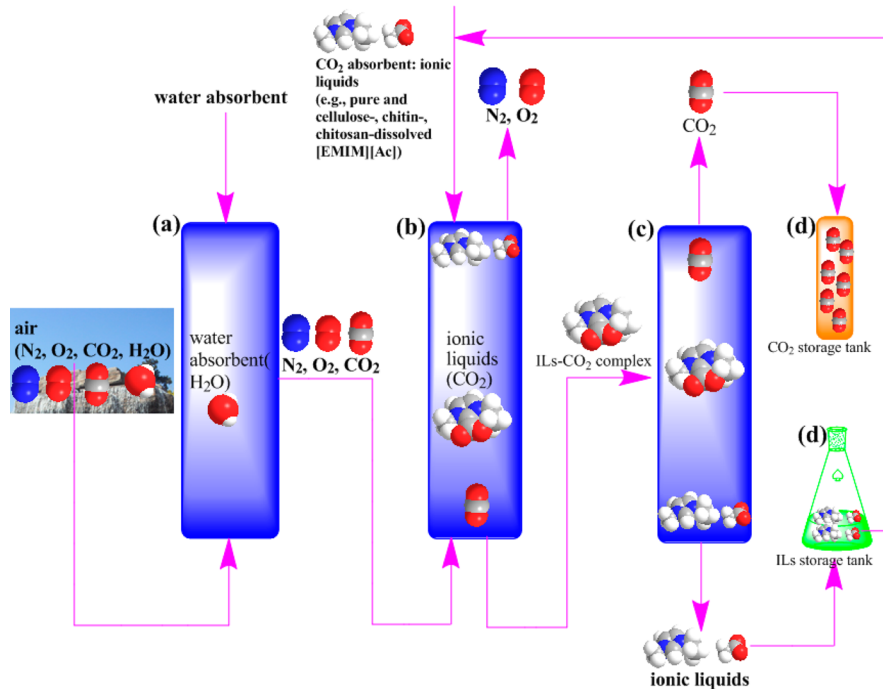


Figure 6. Proposed chemical engineering process for CO₂ absorption and desorption by ILs (e.g., [EMIM][Ac] investigated here) from the atmosphere: water removal by water absorbent (a), CO₂ absorption by ILs (b), CO₂ desorption by reduced pressure or high temperature (c), CO₂ and IL storage (d). Only the main components of air, i.e., N₂, O₂, CO₂, and H₂O, are presented above for the purpose of a better illustration and analysis. The color of the atoms corresponds to the specific atom as follows: N (blue), O (red), C (gray), H (white).

(mol. fra.) % by 45% would obtain the CO₂ capacity in [EMIM][Ac], i.e., 0.35 (mol. fra.) % or 0.09 (mass ratio) % or 900 ppm, contributing to ca. 4% of the overall mass increase. Subtracting 0.09 (mass ratio) % of CO₂ sorption from the overall mass gain 2.27 (mass ratio) % would obtain the mass ratio of neat water to [EMIM][Ac], i.e., 2.18 (mass ratio) %, corresponding to ca. 96% of the overall mass gain. It indicates that CO₂ capture from air by [EMIM][Ac] is fairly limited (only ca. 900 ppm), which might be much (ca. 24 times) lower than water sorption. It is expected that CO₂ uptake in mixtures of [EMIM][Ac] with chitosan or chitin would be greater than that in pure [EMIM][Ac] due to the presence of a NH₂ group.^{71,74,75,79} The increase in the peak area ratio of CO_{2,chem} to OH_b ([EMIM][Ac] with chitosan > [EMIM][Ac] with chitin > [EMIM][Ac] with cellulose > pure [EMIM][Ac]) in Figure 4f corroborates this expectation. The highest atmospheric CO₂ capture in the mixture of [EMIM][Ac] with chitosan also competes with the highest atmospheric water sorption capacity.

Other atmospheric gases (e.g., O₂, N₂, Ar, and CH₄) in [EMIM][Ac] have a negligible solubility in ILs when compared to that of CO₂ and H₂O.^{91,97} Let us take N₂ (ca. 78.084 vol. fra. %) as an example to illustrate this thought. For [EMIM][Ac], the CO₂/N₂ separation factor is as much as 445,⁹¹ indicating a negligible N₂ absorption from air compared to CO₂. Furthermore, the CO₂/N₂ separation factor in [EMIM][Ac] is much higher than that in conventional ILs, such as 14.4 for [BMIM][Tf₂N] and 26.5 for [BMIM][BF₄]. That is to say, [EMIM][Ac] is more promising to selectively capture CO₂ from the air than conventional ILs. It is understandable because the interaction between [EMIM][Ac] and CO₂ is mainly chemisorption,^{48,83} while only weakly physical interaction occurs in the CO₂ sorption in conventional ILs.^{73,97} Normally, capturing CO₂ from air by ILs (e.g., [EMIM][Ac]) contains at

least four procedures: removing water (Figure 6a), absorbing CO₂ (Figure 6b), desorbing CO₂ (Figure 6c), and CO₂ storage (Figure 6d). The details could be seen in section S3 of the Supporting Information.

4. CONCLUSION

The following conclusions were obtained by our investigations.

The atmospheric water dynamic sorption process in pure [EMIM][Ac] and mixtures of [EMIM][Ac] with chitin, cellulose, and chitosan shows a two-regime tendency, a three-regime tendency but accompanied with an unclear indiscernible regime 3, a three-regime tendency but accompanied with an indiscernible regime 2, and a clear three-regime tendency, respectively. The unusually greater hygroscopicity of the mixture of [EMIM][Ac] with chitosan indicates a high possibility of being used as drying materials.

All of the four systems investigated could absorb a trace amount of CO₂ from the air physically, and react with more CO₂ from the air chemically. The chemical CO₂ capture from air by pure [EMIM][Ac] is approximately 0.09 (mass ratio) % g/g CO₂/IL. The CO₂ solubility in [EMIM][Ac] decreases about 50% when the system is exposed to the atmospheric air for a specific time period. It is the first report on the effect of atmospheric water on the dissolution of CO₂ in [EMIM][Ac]. Further work is needed to make it clearer. CO₂ capture from air by ILs is the state-of-the-art research. A more detailed description can be seen in section S4 in the Supporting Information.

ASSOCIATED CONTENT

Supporting Information

Sections describing details for section 3.1 of the manuscript (i.e., Section S0), some prerequisite knowledge and discussions for section 3.4 of the manuscript (i.e., Section S1), comparison

of atmospheric water sorption in [EMIM][Ac] and [BMIM]-[Ac] (i.e., Section S2), the proposed chemical engineering process to capture CO₂ by ILs from air (i.e., Section S3), and conclusion of CO₂ capture by ILs from air (i.e., Section S4). Schemes showing the proposed atmospheric water sorption process in the mixtures of [EMIM][Ac] with chitin (Scheme S1) and chitosan (Scheme S2), Figures showing original, difference, selected second-derivative (Figure S1), s-G-2D-COS, as-G-2D-COS ATR-IR spectra (Figure S2), Mulliken atomic charge distribution (Figure S3), and shift of IR peak position (Figure S4). This material is available free of charge via the Internet at <http://pubs.acs.org>.

AUTHOR INFORMATION

Corresponding Author

*Phone: +86-10-62514925. Fax: +86-10-62516444. E-mail: tcmu@chem.ruc.edu.cn.

Notes

The authors declare no competing financial interest.

ACKNOWLEDGMENTS

This work was supported by the National Natural Science Foundation of China (21173267, 21473252). The authors also thank Professor Morita and Professor Ozaki for the help on obtaining PCMW2D-COS with the software 2D shige.

REFERENCES

- (1) Greaves, T. L.; Drummond, C. J. Protic Ionic Liquids: Properties and Applications. *Chem. Rev.* **2008**, *108*, 206–237.
- (2) Swatloski, R. P.; Spear, S. K.; Holbrey, J. D.; Rogers, R. D. Dissolution of Cellulose with Ionic Liquids. *J. Am. Chem. Soc.* **2002**, *124*, 4974–4975.
- (3) Cui, G. K.; Zheng, J. J.; Luo, X. Y.; Lin, W. J.; Ding, F.; Li, H. R.; Wang, C. M. Tuning Anion-Functionalized Ionic Liquids for Improved SO₂ Capture. *Angew. Chem., Int. Ed.* **2013**, *52*, 10620–10624.
- (4) Wang, C.; Luo, X.; Luo, H.; Jiang, D.; Li, H.; Dai, S. Tuning the Basicity of Ionic Liquids for Equimolar CO₂ Capture. *Angew. Chem., Int. Ed.* **2011**, *50*, 4918–4922.
- (5) Chen, Y.; Cao, Y.; Mu, T. A New Application of Acetate-Based Ionic Liquids: Potential Usage as Drying Materials. *Chem. Eng. Technol.* **2014**, *37*, 1–9.
- (6) Kang, X. C.; Zhang, J. L.; Shang, W. T.; Wu, T. B.; Zhang, P.; Han, B. X.; Wu, Z. H.; Mo, G.; Xing, X. Q. One-Step Synthesis of Highly Efficient Nanocatalysts on the Supports with Hierarchical Pores Using Porous Ionic Liquid-Water Gel. *J. Am. Chem. Soc.* **2014**, *136*, 3768–3771.
- (7) Blanchard, L. A.; Hancu, D.; Beckman, E. J.; Brennecke, J. F. Green Processing Using Ionic Liquids and CO₂. *Nature* **1999**, *399*, 28–29.
- (8) Xue, Z.; Zhang, Z.; Han, J.; Chen, Y.; Mu, T. Carbon Dioxide Capture by a Dual Amino Ionic Liquid with Amino-functionalized Imidazolium Cation and Taurine Anion. *Int. J. Greenhouse Gas Control* **2011**, *5*, 628–633.
- (9) Cheng, X.; Mu, T.; Wang, X.; Guo, X.; Zou, L. Low Pressure Solubilities of Vinyl Chloride in Ionic Liquid. *J. Chem. Eng. Data* **2008**, *53*, 2807–2809.
- (10) Cheng, X.; Yang, G.; Mu, T.; Guo, X.; Wang, X. Absorption of Vinyl Chloride by Room Temperature Ionic Liquids. *Clean: Soil, Air, Water* **2009**, *37*, 245–248.
- (11) Wu, W.; Han, B.; Gao, H.; Liu, Z.; Jiang, T.; Huang, J. Desulfurization of Flue Gas: SO₂ Absorption by an Ionic Liquid. *Angew. Chem., Int. Ed.* **2004**, *43*, 2415–2417.
- (12) Palomar, J.; Gonzalez-Miquel, M.; Bedia, J.; Rodriguez, F.; Rodriguez, J. J. Task-specific Ionic Liquids for Efficient Ammonia Absorption. *Sep. Purif. Technol.* **2011**, *82*, 43–52.
- (13) Zhao, Y.; Yu, B.; Yang, Z.; Zhang, H.; Hao, L.; Gao, X.; Liu, Z. A Protic Ionic Liquid Catalyzes CO₂ Conversion at Atmospheric Pressure and Room Temperature: Synthesis of Quinazoline-2,4-(1H,3H)-diones. *Angew. Chem., Int. Ed.* **2014**, *53*, 5922–5925.
- (14) Luo, X. Y.; Guo, Y.; Ding, F.; Zhao, H. Q.; Cui, G. K.; Li, H. R.; Wang, C. M. Significant Improvements in CO₂ Capture by Pyridine-Containing Anion-Functionalized Ionic Liquids through Multiple-Site Cooperative Interactions. *Angew. Chem., Int. Ed.* **2014**, *53*, 7053–7057.
- (15) Wang, C.; Cui, G.; Luo, X.; Xu, Y.; Li, H.; Dai, S. Highly efficient and reversible SO₂ capture by tunable azole-based ionic liquids through multiple-site chemical absorption. *J. Am. Chem. Soc.* **2011**, *133*, 11916–11919.
- (16) Wang, C.; Luo, H.; Jiang, D.; Li, H.; Dai, S. Carbon Dioxide Capture by Superbase Derived Protic Ionic Liquids. *Angew. Chem., Int. Ed.* **2010**, *122*, 6114–6117.
- (17) Cao, Y.; Chen, Y.; Mu, T. A New Way to Tune Relative Humidity: by Saturated Ionic Liquid Aqueous Solutions. *New J. Chem.* **2013**, *37*, 3890–3898.
- (18) Yan, C.; Mu, T. Investigation of Ionic Liquids for Efficient Removal and Reliable Storage of Radioactive Iodine: a Halogen-bonding Case. *Phys. Chem. Chem. Phys.* **2014**, *16*, 5071–5075.
- (19) Barber, P. S.; Griggs, C. S.; Gurau, G.; Liu, Z.; Li, S.; Li, Z.; Lu, X.; Zhang, S.; Rogers, R. D. Coagulation of Chitin and Cellulose from 1 - Ethyl - 3 - methylimidazolium Acetate Ionic - Liquid Solutions Using Carbon Dioxide. *Angew. Chem., Int. Ed.* **2013**, *125*, 12576–12579.
- (20) Zhang, H.; Wu, J.; Zhang, J.; He, J. 1-Allyl-3-Methylimidazolium Chloride Room Temperature Ionic Liquid: A New and Powerful Nondemulsifying Solvent for Cellulose. *Macromolecules* **2005**, *38*, 8272–8277.
- (21) Wu, Y.; Sasaki, T.; Irie, S.; Sakurai, K. A Novel Biomass-Ionic Liquid Platform for the Utilization of Native Chitin. *Polymer* **2008**, *49*, 2321–2327.
- (22) Gupta, K. M.; Hu, Z.; Jiang, J. Molecular Insight into Cellulose Regeneration from a Cellulose/Ionic liquid Mixture: Effects of Water Concentration and Temperature. *RSC Adv.* **2013**, *3*, 4425–4433.
- (23) Huo, F.; Liu, Z.; Wang, W. Cosolvent or Antisolvent? A Molecular View of the Interface Between Ionic Liquids and Cellulose upon Addition of Another Molecular Solvent. *J. Phys. Chem. B* **2013**, *117*, 11780–11792.
- (24) Zhao, Y.; Liu, X.; Wang, J.; Zhang, S. Insight into the Cosolvent Effect of Cellulose Dissolution in Imidazolium-Based Ionic Liquid Systems. *J. Phys. Chem. B* **2013**, *117*, 9042–9049.
- (25) Aparicio, S.; Alcalde, R.; Attilhan, M. Experimental and Computational Study on the Properties of Pure and Water Mixed 1-Ethyl-3-Methylimidazolium L-(+)-Lactate Ionic Liquid. *J. Phys. Chem. B* **2010**, *114*, 5795–5809.
- (26) Anthony, J. L.; Maginn, E. J.; Brennecke, J. F. Solution Thermodynamics of Imidazolium-Based Ionic Liquids and Water. *J. Phys. Chem. B* **2001**, *105*, 10942–10949.
- (27) Seddon, K. R.; Stark, A.; Torres, M. J. Influence of Chloride, Water, and Organic Solvents on the Physical Properties of Ionic Liquids. *Pure Appl. Chem.* **2000**, *72*, 2275–2287.
- (28) Cuadrado-Prado, S.; Dominguez-Perez, M.; Rilo, E.; Garcia-Garabal, S.; Segade, L.; Franjo, C.; Cabeza, O. Experimental Measurement of the Hygroscopic Grade on Eight Imidazolium Based Ionic Liquids. *Fluid Phase Equilib.* **2009**, *278*, 36–40.
- (29) Cammarata, L.; Kazarian, S.; Salter, P.; Welton, T. Molecular States of Water in Room Temperature Ionic Liquids. *Phys. Chem. Chem. Phys.* **2001**, *3*, 5192–5200.
- (30) Lovelock, K. R. J.; Smith, E. F.; Deyko, A.; Villar-Garcia, I. J.; Licence, P.; Jones, R. G. Water Adsorption on a Liquid Surface. *Chem. Commun.* **2007**, 4866–4868.
- (31) Tran, C. D.; Lacerda, S. H. D.; Oliveira, D. Absorption of Water by Room-Temperature Ionic Liquids: Effect of Anions on Concentration and State of Water. *Appl. Spectrosc.* **2003**, *57*, 152–157.
- (32) Restolho, J.; Mata, J. L.; Colaço, R.; Saramago, B. J. Moisture Absorption in Ionic Liquid Films. *J. Phys. Chem. C* **2013**, *117*, 10454–10463.

- (33) Di Francesco, F.; Calisi, N.; Creatini, M.; Melai, B.; Salvo, P.; Chiappe, C. Water Sorption by Anhydrous Ionic Liquids. *Green Chem.* **2011**, *13*, 1712–1717.
- (34) Cao, Y.; Chen, Y.; Sun, X.; Zhang, Z.; Mu, T. Water Sorption in Ionic Liquids: Kinetics, Mechanisms and Hydrophilicity. *Phys. Chem. Chem. Phys.* **2012**, *14*, 12252–12262.
- (35) Cao, Y.; Chen, Y.; Wang, X.; Mu, T. Predicting the Hygroscopicity of Imidazolium-Based ILs Varying in Anion by Hydrogen-Bonding Basicity and Acidity. *RSC Adv.* **2014**, *4*, 5169–5176.
- (36) Freire, M. G.; Neves, C. M. S. S.; Marrucho, I. M.; Coutinho, J. A. P.; Fernandes, A. M. Hydrolysis of Tetrafluoroborate and Hexafluorophosphate Counter Ions in Imidazolium-Based Ionic Liquids. *J. Phys. Chem. A* **2010**, *114*, 3744–3749.
- (37) Mele, A.; Tran, C. D.; De Paoli Lacerda, S. H. The Structure of a Room-Temperature Ionic Liquid with and without Trace Amounts of Water: The Role of C - H···O and C - H···F Interactions in 1-N-Butyl-3-Methylimidazolium Tetrafluoroborate. *Angew. Chem., Int. Ed.* **2003**, *115*, 4500–4502.
- (38) Takamuku, T.; Kyoshin, Y.; Shimomura, T.; Kittaka, S.; Yamaguchi, T. Effect of Water on Structure of Hydrophilic Imidazolium-Based Ionic Liquid. *J. Phys. Chem. B* **2009**, *113*, 10817–10824.
- (39) Saha, S.; Hamaguchi, H.-o. Effect of Water on the Molecular Structure and Arrangement of Nitrile-Functionalized Ionic Liquids. *J. Phys. Chem. B* **2006**, *110*, 2777–2781.
- (40) Li, W.; Zhang, Z.; Han, B.; Hu, S.; Xie, Y.; Yang, G. Effect of Water and Organic Solvents on the Ionic Dissociation of Ionic Liquids. *J. Phys. Chem. B* **2007**, *111*, 6452–6456.
- (41) Jiang, W.; Wang, Y.; Voth, G. A. Molecular Dynamics Simulation of Nanostructural Organization in Ionic Liquid/Water Mixtures. *J. Phys. Chem. B* **2007**, *111*, 4812–4818.
- (42) Brehm, M.; Weber, H.; Pensado, A. S.; Stark, A.; Kirchner, B. Proton Transfer and Polarity Changes in Ionic Liquid–Water Mixtures: A Perspective on Hydrogen Bonds from *ab initio* Molecular Dynamics at the Example of 1-Ethyl-3-Methylimidazolium Acetate–Water Mixtures—Part 1. *Phys. Chem. Chem. Phys.* **2012**, *14*, 5030–5044.
- (43) Fendt, S.; Padmanabhan, S.; Blanch, H. W.; Prausnitz, J. M. Viscosities of Acetate or Chloride-Based Ionic Liquids and Some of Their Mixtures with Water or Other Common Solvents. *J. Chem. Eng. Data* **2010**, *S6*, 31–34.
- (44) Quijada-Maldonado, E.; van der Boogaart, S.; Lijbers, J.; Meindersma, G.; de Haan, A. Experimental Densities, Dynamic Viscosities and Surface Tensions of the Ionic Liquids Series 1-Ethyl-3-Methylimidazolium Acetate and Dicyanamide and Their Binary and Ternary Mixtures with Water and Ethanol at T = (298.15 to 343.15 K). *J. Chem. Thermodyn.* **2012**, *51*, 51–58.
- (45) Hall, C. A.; Le, K. A.; Rudaz, C.; Radhi, A.; Lovell, C. S.; Damion, R. A.; Budtova, T.; Ries, M. E. Macroscopic and Microscopic Study of 1-Ethyl-3-Methyl-Imidazolium Acetate–Water Mixtures. *J. Phys. Chem. B* **2012**, *116*, 12810–12818.
- (46) Shi, W.; Nulwala, H.; Achary, D. K.; Luebke, D. R. Theoretical and Experimental Studies of Water Interaction in Acetate Based Ionic Liquids. *Phys. Chem. Chem. Phys.* **2012**, *14*, 15897–15908.
- (47) Stevanovic, S.; Podgoršek, A.; Pádua, A. A. H.; Costa Gomes, M. F. Effect of Water on the Carbon Dioxide Absorption by 1-Alkyl-3-Methylimidazolium Acetate Ionic Liquids. *J. Phys. Chem. B* **2012**, *116*, 14416–14425.
- (48) Besnard, M.; Cabaço, M. I.; Chávez, F. V.; Pinaud, N.; Sebastião, P. J.; Coutinho, J. A.; Danten, Y. On the Spontaneous Carboxylation of 1-Butyl-3-Methylimidazolium Acetate by Carbon Dioxide. *Chem. Commun.* **2012**, *48*, 1245–1247.
- (49) Barrosse-Antle, L. E.; Compton, R. G. Reduction of Carbon Dioxide In 1-Butyl-3-Methylimidazolium Acetate. *Chem. Commun.* **2009**, *3744*–3746.
- (50) Shiflett, M. B.; Drew, D. W.; Cantini, R. A.; Yokozeki, A. Carbon Dioxide Capture Using Ionic Liquid 1-Butyl-3-Methylimidazolium Acetate. *Energy Fuels* **2010**, *24*, 5781–5789.
- (51) Shiflett, M. B.; Kasprzak, D. J.; Junk, C. P.; Yokozeki, A. Phase Behavior of {Carbon Dioxide+[bmim][Ac]} Mixtures. *J. Chem. Thermodyn.* **2008**, *40*, 25–31.
- (52) Lackner, K. S.; Grimes, P.; Ziock, H.-J. Capturing Carbon Dioxide from Air. In *First National Conference on Carbon Sequestration, Washington, DC*, 2001.
- (53) Stolaroff, J. K.; Keith, D. W.; Lowry, G. V. Carbon Dioxide Capture from Atmospheric Air Using Sodium Hydroxide Spray. *Environ. Sci. Technol.* **2008**, *42*, 2728–2735.
- (54) Choi, S.; Drese, J. H.; Eisenberger, P. M.; Jones, C. W. Application of Amine-Tethered Solid Sorbents for Direct CO₂ Capture from the Ambient Air. *Environ. Sci. Technol.* **2011**, *45*, 2420–2427.
- (55) Goepert, A.; Czaun, M.; Prakash, G. S.; Olah, G. A. Air as the Renewable Carbon Source of the Future: An Overview of CO₂ Capture from the Atmosphere. *Energy Environ. Sci.* **2012**, *5*, 7833–7853.
- (56) Noda, I. Two-Dimensional Infrared (2D IR) Spectroscopy: Theory and Applications. *Appl. Spectrosc.* **1990**, *44*, 550–561.
- (57) Noda, I. Generalized Two-Dimensional Correlation Method Applicable to Infrared, Raman, and Other Types of Spectroscopy. *Appl. Spectrosc.* **1993**, *47*, 1329–1336.
- (58) Noda, I. Two-Dimensional Infrared Spectroscopy. *J. Am. Chem. Soc.* **1989**, *111*, 8116–8118.
- (59) Thomas, M.; Richardson, H. H. Two-Dimensional FT-IR Correlation Analysis of the Phase Transitions in a Liquid Crystal, 4'-N-Octyl-4-Cyanobiphenyl (8CB). *Vib. Spectrosc.* **2000**, *24*, 137–146.
- (60) Morita, S.; Shinzawa, H.; Noda, I.; Ozaki, Y. Perturbation-Correlation Moving-Window Two-Dimensional Correlation Spectroscopy. *Appl. Spectrosc.* **2006**, *60*, 398–406.
- (61) Morita, S.; Shinzawa, H.; Tsenkova, R.; Noda, I.; Ozaki, Y. Computational Simulations and a Practical Application of Moving-Window Two-Dimensional Correlation Spectroscopy. *J. Mol. Struct.* **2006**, *799*, 111–120.
- (62) Sun, B.; Jin, Q.; Tan, L.; Wu, P.; Yan, F. Trace of the Interesting "V"-Shaped Dynamic Mechanism of Interactions between Water and Ionic Liquids. *J. Phys. Chem. B* **2008**, *112*, 14251–14259.
- (63) Sun, B.; Wu, P. Trace of the Thermally Induced Evolution Mechanism of Interactions between Water and Ionic Liquids. *J. Phys. Chem. B* **2010**, *114*, 9209–9219.
- (64) Andanson, J.-M.; Jutz, F.; Baiker, A. Investigation of Binary and Ternary Systems of Ionic Liquids with Water and/or Supercritical CO₂ by *in situ* Attenuated Total Reflection Infrared Spectroscopy. *J. Phys. Chem. B* **2010**, *114*, 2111–2117.
- (65) Morita, S.; Shinzawa, H.; Noda, I.; Ozaki, Y. Effect of band position shift on moving-window two-dimensional correlation spectroscopy. *J. Mol. Struct.* **2006**, *799*, 16–22.
- (66) Richardson, H. H. 2D-IR correlation and principle component analysis of interfacial melting of thin ice films. *J. Mol. Struct.* **2006**, *799*, 56–60.
- (67) Chen, Y.; Cao, Y.; Lu, X.; Zhao, C.; Yan, C.; Mu, T. Water Sorption in Protic Ionic Liquids: Correlation between Hygroscopicity and Polarity. *New J. Chem.* **2013**, *37*, 1959–1967.
- (68) Cao, Y.; Sun, X.; Chen, Y.; Mu, T. Water Sorption in Amino-Acid Ionic Liquids: Kinetic, Mechanism, and Correlations between Hygroscopicity and Solvatochromic Parameters. *ACS Sustainable Chem. Eng.* **2013**, *2*, 138–148.
- (69) Cao, Y.; Chen, Y.; Lu, L.; Xue, Z.; Mu, T. Water Sorption in Functionalized Ionic Liquids: Kinetics and Intermolecular Interactions. *Ind. Eng. Chem. Res.* **2013**, *52*, 2073–2083.
- (70) Yamaguchi, Y.; Nge, T. T.; Takemura, A.; Hori, N.; Ono, H. Characterization of Uniaxially Aligned Chitin Film by 2D FT-IR Spectroscopy. *Biomacromolecules* **2005**, *6*, 1941–1947.
- (71) Xie, H.; Zhang, S.; Li, S. Chitin and Chitosan Dissolved in Ionic Liquids as Reversible Sorbents of CO₂. *Green Chem.* **2006**, *8*, 630–633.
- (72) Minke, R.; Blackwell, J. The Structure of α -Chitin. *J. Mol. Biol.* **1978**, *120*, 167–181.

- (73) Blanchard, L. A.; Gu, Z.; Brennecke, J. F. High-Pressure Phase Behavior of Ionic Liquid/CO₂ Systems. *J. Phys. Chem. B* **2001**, *105*, 2437–2444.
- (74) Bates, E. D.; Mayton, R. D.; Ntai, I.; Davis, J. H. CO₂ Capture by a Task-Specific Ionic Liquid. *J. Am. Chem. Soc.* **2002**, *124*, 926–927.
- (75) Zhang, S. J.; Zhang, J. M.; Dong, K.; Zhang, Y. Q.; Shen, Y. Q.; Lv, X. M. Supported Absorption of CO₂ by Tetrabutylphosphonium Amino Acid Ionic Liquids. *Chem.—Eur. J.* **2006**, *12*, 4021–4026.
- (76) Zhang, Y.; Zhang, S.; Lu, X.; Zhou, Q.; Fan, W.; Zhang, X. P. Dual Amino Functionalised Phosphonium Ionic Liquids for CO₂ Capture. *Chem.—Eur. J.* **2009**, *15*, 3003–3011.
- (77) Zhang, X.; Dong, H.; Zhao, Z.; Zhang, S.; Huang, Y. Carbon Capture with Ionic Liquids: Overview and Progress. *Energy Environ. Sci.* **2012**, *5*, 6668–6681.
- (78) Tang, J.; Sun, W.; Tang, H.; Radosz, M.; Shen, Y. Enhanced CO₂ Absorption of Poly(ionic liquid)s. *Macromolecules* **2005**, *38*, 2037–2039.
- (79) Schneider, W. F.; Gurkan, B. E.; de la Fuente, J. C.; Mindrup, E. M.; Ficke, L. E.; Goodrich, B. F.; Price, E. A.; Brennecke, J. F. Equimolar CO₂ Absorption by Anion-Functionalized Ionic Liquids. *J. Am. Chem. Soc.* **2010**, *132*, 2116–2117.
- (80) Yokozeki, A.; Shiflett, M. B.; Junk, C. P.; Grieco, L. M.; Foo, T. Physical and Chemical Absorptions of Carbon Dioxide in Room-Temperature Ionic Liquids. *J. Phys. Chem. B* **2008**, *112*, 16654–16663.
- (81) Shiflett, M. B.; Yokozeki, A. Phase Behavior of Carbon Dioxide in Ionic Liquids: [emim][acetate], [emim][trifluoroacetate], and [emim][acetate] plus [emim][trifluoroacetate] Mixtures. *J. Chem. Eng. Data* **2009**, *54*, 108–114.
- (82) Chen, Y.; Han, J.; Wang, T.; Mu, T. Determination of Absorption Rate and Capacity of CO₂ in Ionic Liquids at Atmospheric Pressure by Thermogravimetric Analysis. *Energy Fuels* **2011**, *25*, 5810–5815.
- (83) Gurau, G.; Rodríguez, H.; Kelley, S. P.; Janiczek, P.; Kalb, R. S.; Rogers, R. D. Demonstration of Chemisorption of Carbon Dioxide in 1, 3-Dialkylimidazolium Acetate Ionic Liquids. *Angew. Chem., Int. Ed.* **2011**, *50*, 12024–12026.
- (84) Angamuthu, R.; Byers, P.; Lutz, M.; Spek, A. L.; Bouwman, E. Electrocatalytic CO₂ Conversion to Oxalate by a Copper Complex. *Science* **2010**, *327*, 313–315.
- (85) Keith, D. W. Why Capture CO₂ from the Atmosphere? *Science* **2009**, *325*, 1654–1655.
- (86) Zeman, F. S.; Lackner, K. S. Capturing Carbon Dioxide Directly from the Atmosphere. *Water Resour. Res.* **2004**, *16*, 157–172.
- (87) Zeman, F. Experimental Results for Capturing CO₂ from the Atmosphere. *AIChE J.* **2008**, *54*, 1396–1399.
- (88) Stuckert, N. R.; Yang, R. T. CO₂ Capture from the Atmosphere and Simultaneous Concentration Using Zeolites and Amine-Grafted SBA-15. *Environ. Sci. Technol.* **2011**, *45*, 10257–10264.
- (89) Hansen, J.; Sato, M.; Kharecha, P.; Beerling, D.; Berner, R.; Masson-Delmotte, V.; Pagani, M.; Raymo, M.; Royer, D. L.; Zachos, J. C. Target Atmospheric CO₂: Where Should Humanity Aim? *Open Atmos. Sci. J.* **2008**, *2*, 217–231.
- (90) Huddleston, J. G.; Visser, A. E.; Reichert, W. M.; Willauer, H. D.; Broker, G. A.; Rogers, R. D. Characterization and Comparison of Hydrophilic and Hydrophobic Room Temperature Ionic Liquids Incorporating the Imidazolium Cation. *Green Chem.* **2001**, *3*, 156–164.
- (91) Blath, J.; Deubler, N.; Hirth, T.; Schiestel, T. Chemisorption of Carbon Dioxide in Imidazolium Based Ionic Liquids with Carboxylic Anions. *Chem. Eng. J.* **2012**, *181*, 152–158.
- (92) Cabaço, M. I.; Besnard, M.; Danten, Y.; Coutinho, J. Carbon Dioxide in 1-Butyl-3-Methylimidazolium Acetate. I. Unusual Solubility Investigated by Raman Spectroscopy and DFT Calculations. *J. Phys. Chem. A* **2012**, *116*, 1605–1620.
- (93) Besnard, M.; Cabaço, M. I.; Vaca Chávez, F. n.; Pinaud, N. l.; Sebastião, P. J.; Coutinho, J. o. A.; Mascetti, J. l.; Danten, Y. CO₂ in 1-Butyl-3-Methylimidazolium Acetate. 2. NMR Investigation of Chemical Reactions. *J. Phys. Chem. A* **2012**, *116*, 4890–4901.
- (94) Carvalho, P. J.; Álvarez, V. H.; Schröder, B.; Gil, A. M.; Marrucho, I. M.; Aznar, M.; Santos, L.; Coutinho, J. A. P. Specific Solvation Interactions of CO₂ on Acetate and Trifluoroacetate Imidazolium Based Ionic Liquids at High Pressures. *J. Phys. Chem. B* **2009**, *113*, 6803–6812.
- (95) Maginn, E. J. *Design and Evaluation of Ionic Liquids as Novel CO₂ Absorbents*; National Energy Technology Laboratory: US, 2004.
- (96) Rodríguez, H.; Gurau, G.; Holbrey, J. D.; Rogers, R. D. Reaction of Elemental Chalcogens with Imidazolium Acetates to Yield Imidazole-2-Chalcogenones: Direct Evidence for Ionic Liquids as Proto-Carbenes. *Chem. Commun.* **2011**, *47*, 3222–3224.
- (97) Anderson, J. L.; Dixon, J. N. K.; Brennecke, J. F. Solubility of CO₂, CH₄, C₂H₆, C₂H₄, O₂, and N₂ in 1-Hexyl-3-Methylpyridinium Bis (trifluoromethylsulfonyl) imide: Comparison to other Ionic Liquids. *Acc. Chem. Res.* **2007**, *40*, 1208–1216.